Study on Cyclohexyl isocyanate-modified Graphene and Mechanical,Thermal and Tribological Properties of its Polyimide Nanocomposite

DUXIN LI*, YUE CHEN, WENYAN YANG, CHUNGUANG XIAO AND MENGLIN WEI

State Key Laboratory of Powder Metallurgy, Central South University, Changsha 410083, China

ABSTRACT

To elucidate the effect and the mechanism of graphene modification on the morphology and properties of polyimide (PI), cyclohexyl isocyanate modified graphene (CG), was designed and prepared by grafting the isocyanate chain on the graphene sheet surface, followed by the use of the modified graphene for the preparation of polyimide composites by in situ polymerization. The successful grafting of cyclohexyl isocyanate onto the surface of the graphene was confirmed by Fourier transform infrared spectroscopy, X-ray diffraction, and Raman spectroscopy. The unique surface modification significantly improved the compatibility and dispersion of graphene in the PI matrix. CG/polyimide composites were prepared by in situ polymerization. The tensile strength and Young's modulus of the 1.0CG/PI nanocomposite reached 99.35 MPa and 1.84 GPa, showing increases of 20.97 % and 28.67 %, respectively, compared to the values of pure PI. The friction coefficient of the 1.0CG/PI composite reached 0.35, i.e., it was 32.69 % lower than that of pure PI, and the wear rate was reduced by 29.10 %. This improvement of the tribological properties was mainly caused by the cooperative interaction of the mechanical and thermal properties of the composites and the high self-lubricity of modified graphene.

KEYWORDS: *Cyclohexyl isocyanate, Graphene, Polyimide, Thermal properties, Mechanical properties, Tribological mechanism*

INTRODUCTION

Among the different polymers, owing to its unique high temperature resistance, mechanical properties, tribological properties and dielectric properties, polyimide (PI) is widely used in aviation, aerospace engineering, microelectronics and several other fields [1-6]. Bearings, gears, seals, and friction plates are often made from PI materials [7, 8]. In particular,

J. Polym. Mater. Vol. **35,** No. 1, 2018, 119-136

Correspondence author e-mail: liduxin6404@csu.edu.cn

PI coatings are used in high-speed engines as an anti-wear lubrication layer between the piston wall and cylinder wall, effectively reducing the friction coefficient and prolonging the service life of some industrial components. However, the tribological performance of PI is not enough to meet the severe demands in some aerospace mechanical parts. Therefore, since the rapid development of PI in 1950s, the modification of PI materials has been of great interest and has been studied by the polymer industry and academic research groups worldwide[9-15]. Among the PI modifications, the use of a hybridization matrix with fillers is an inexpensive, facile, and common method. In previous studies, nano- and micro-scale fillers such as sericite, molybdenum disulphide, graphene carbon, nanobars and carbon nanotubes, have been successfully used to improve the performance of PI [16-21].

Graphene, as the material with the highest potential to change the world in the twenty-first century, has high electrical conductivity, thermal conductivity, lubricity, flame retardancy and excellent mechanical properties [22-26]. Since it was first prepared by the Geim group in Manchester University via the micromechanical stripping method in 2004 [27], the modification of polymer materials by graphene has been highly promising, and increasing amounts of attention have been devoted to this area. However, because graphene can easily reassemble with itself and interacts weakly with polymers, surface modification of graphene is the first issue that must be addressed to improve the dispersion and compatibility of graphene in a polymer matrix and enable the exploitation of the advantages of graphene/ polymer composites [28-31].

Several research groups have followed the approach of choosing active molecules such as silane coupling agents, amines, and surfactants for graphene modification [32-36]. On the other hand, there are few reports on the modification of graphene by isocyanate, which shows stronger chemical activity and requires milder reaction conditions. The groups of Lin[37] and Li [38] choose toluene-2,4-diisocyanate and tri-isocyanate, respectively, as modifiers, prepared the isocyanate modified graphene, and found that the surface of the graphene sheets changes from hydrophilic to hydrophobic and that some properties of the sheets were enhanced. However, the cyclohexyl isocyanate has not so far been considered and discussed. Cyclohexyl isocyanate (CI) has a simple and stable structure and a low cost and is a special sort of isocyanate with a stable and bulky six-membered ring. It is expected that after being inserted into the graphite layers, it could increase the spacing between the layers and improve the exfoliation and dispersion of graphene. Stankovich et al.[39] prepared the cyclohexyl isocyanate modified graphene and found that it could form a stable dispersion in polar aprotic solvents. Nevertheless, the modification of cyclohexyl isocyanate still requires further study, and the application performances of cyclohexyl isocyanate/ polymer composites also must be investigated. A few groups[40-42] have investigated isocyanate-modified graphene/ polymer composites, but some issues, including the properties and modification mechanism, still need to be discussed further, and the tribological performance characteristics of cyclohexyl isocyanate

modified graphene/ PI composites have been rarely reported in the past.

With this in mind, in this work, we designed and prepared the cyclohexyl isocyanate modified graphene (CG) and systematically investigated the grafting effect and the properties of modified graphene. We then prepared CG/PI composites and evaluated the mechanical and thermal properties of polyimide composite. The tribological properties of CG/PI nanocomposite films were measured by a ball-on-disc tribotester under dry-slide conditions. Friction-reducing and anti-wear mechanism of the CG/PI composites were also emphasized and discussed. This study is expected to introduce the studies of graphene/PI composites and broaden the scope of their applications.

EXPERIMENTAL

2.1. Materials

Flake graphite powder (30 μm) was purchased from Yingtai Co., China. Cyclohexyl isocyanate (CI), concentrated sulfuric acid (purity of 98%, AR) and potassium permanganate were purchased from ShenHua Sci. Institute, Changsha, China. Hydrogen peroxide 35%, 4, 4'-(4, 4'-Isopropylidenediphenyl-1,1'-diyldioxy) dianiline (BAPP), 4,4-Diaminodiphenyl methane (MDA), 3, 3', 4, 4'-Benzophenonetetracarboxylic dianhydride (BTDA), and 1-Methyl-2-pyrrolidinone (NMP) were of analytical grade and were from YongFeng Co., DanYang, China. Concentrated hydrochloric acid (35%, AR) obtained from the Hong Hua Company was diluted with deionized water at a 1:10 ratio as received. All other chemical reagents were of commercial analytical grade and were used without further purification.

2.2. Preparation of cyclohexyl isocyanate modified graphene

Graphene oxide (GO) was obtained by the modified Hummer's method of flake graphite (FG) [43], as shown in the Supporting Information (SI). The GO solution was ultrasonically agitated, centrifuged, washed 5 times and freeze-dried. Then, 2 g of the received GO was uniformly dispersed in 200 mL of the NMP solvent prior to ultrasonic vibration for 2 h. A total of 2 mg CI was added dropwise into the mixture, which was then stirred for 48 h at room temperature, filtered and washed 3 times by NMP and ethanol. The product was vacuum-dried at 55 °C and labelled cyclohexyl isocyanate modified graphene (CG).

2.3. Preparation of the CG/polyimide composites

Pure PI and CG/PI films were prepared by in situ polymerization and subsequent thermal imidization (in Fig. 1). Based on the total mass of reactants, the appropriate amount of CG was dispersed ultrasonically in a NMP solution. 2.5 mmol of MDA and 5 mmol BAPP were stirred with the CG/NMP solution obtained as described above. Subsequently, 7.5 mmol of BTDA was divided into the liquor, and the amount of solvent was adjusted to ensure the solid content of PI was 25 wt%. The mixture was vigorously stirred for 24 h at room temperature and became a homogeneous viscous CG and polyamic acid (PAA) liquid. The CG/PAA liquid was painted on glass substrates, placed in a vacuum oven at 80 °C for 2 h to remove air bubbles, and then heated at 100, 150, 200, and 300 °C for 1 h to remove volatiles. Then, CG/PI composites were obtained with 0.2%, 0.5%, 1.0% mass loading of CG, labelled as 0.2CG/PI, 0.5CG/PI, 1.0CG/PI, respectively.

2.4. Characterization

X-ray diffraction (XRD) studies were performed using a DX-2700B (Dandong Radius Instrument Co., Ltd., China) instrument with CuKα radiation (λ=0.154 nm, 0.03°/s) at 40 kV and 250 mA. Fourier transform infrared spectroscopy (FT-IR) was performed using a Nicolet 6700 spectrometer over the range of 4000-400 cm^{-1}. The morphology was observed by a Nova Nano SEM230 (FEI Co., ltd, USA) field-emission scanning electron microscope (SEM) with an acceleration voltage of 20 kV. All surfaces were sputtered with gold to enhance the image resolution and to prevent electrostatic charging. Transmission

electron microscopy (TEM) was performed using a field emission microscope (JEM-JEOL 2100F, Japan), following an aqueous solution of graphene (1.0 mg/ mL) coating on the copper-carbon grid. Atomic force microscopy (AFM, NS3a, Veeco instruments Inc., USA) was employed to detecting the images in the tapping mode after the aqueous solution of graphene obtained as described above was dropped onto a mica sheet. The behaviour of the electrons and phonons of the samples was investigated by Raman spectroscopy (LabRAM HR-800, HORIBA Scientific, France). Thermogravimetric analysis (TGA) was performed by a thermal analyser instrument (NETZSCH STA 449C) at a rate of 10 °C/min from room temperature to 800 °C under the protection of argon gas. Tensile tests were performed by a microcomputer control machine (Instron 3369, America) in accordance with ISO 527-2: 1993 at a tensile rate of 2 mm/min. Friction and wear tests were conducted by a ball-on-disc tribometer (Peseux, Switzerland) at room temperature under dry friction conditions (in Fig. 2), according to Chinese standard GB3960-83 as described in the SI. Experiments for each group of samples were tested at the load of 5 N and the sliding speed of 0.628 m/s and sliding distance of 1500 m. After friction test, the wear trace was observed and measured by a three-dimensional surface profiler (Wyko NT910, USA), with an accuracy of 0.01 mm. The friction coefficients were obtained directly by the tribometer, and the wear volume ΔV (mm^3) was obtained based on the following equation (1):

$$\Delta V\,(mm^3) = B\left[\frac{\pi r^2}{180}\ arcsin\ \left(\frac{w}{2r}\right) - \frac{w}{2}\sqrt{r^2 - \left(\frac{w}{2}\right)^2}\right] \quad (1)$$

where B is the circle of friction (mm), r is the radius of the chromium steel ball (mm), and ω is the width of the wear trace (mm). Finally, the specific wear rate WR (mm^3/ Nm) was calculated from the volume loss by using the following equation:

$$WR\ (mm^3\ /Nm) = \frac{\Delta V}{F \cdot L} \quad (2)$$

Where ΔV is the wear volume loss (mm^3), F is the load (N), L is the sliding distance (m).

3. RESULTS AND DISCUSSION

3.1. Characterization of cyclohexyl isocyanate modified graphene

The preparation of polymer nanocomposites by in situ polymerization, where the reaction monomers can be inserted and polymerized between the layers of the modified graphene, can enhance the dispersion of graphene and the properties of polymer composites. To inhibit the agglomeration and improve the dispersion of graphene in the organic system, the GO was grafted with cyclohexyl isocyanate, and thus, its surface was coated by the hydrophobic groups. After the grafting reaction, a dispersity test within the same standing time was carried out by dispersing GO and CG, respectively, in the NMP solvent, with a concentration of 1.8 mg/mL. It was found that GO can be dispersed evenly within standing time 1 h, but GO precipitation appears obviously within a long period of time (24 h or longer). Within the same standing time, as shown in Fig. 3(c-d), CG can still maintain good dispersion in NMP. This is mainly due to the coating of organic groups and the formation of hydrogen bonds between the amide of CG and the organic solvent, thus increasing the dispersion.

Successful modifying of CI chain on the graphene surface was proved by FT-IR spectra (Fig. 4), which showed the absorption peaks closely relating to the molecular structure and functional groups. The spectra of GO show characteristic peaks at 1050, 1382, 1634, 3414 cm^{-1}, corresponding to the stretching vibrational peaks of the C–O–C groups in epoxy, the C–OH bending vibration, the C=O stretching vibration from the carboxyl group and the –OH stretching vibration, respectively. In addition, some new peaks in CG's spectra,

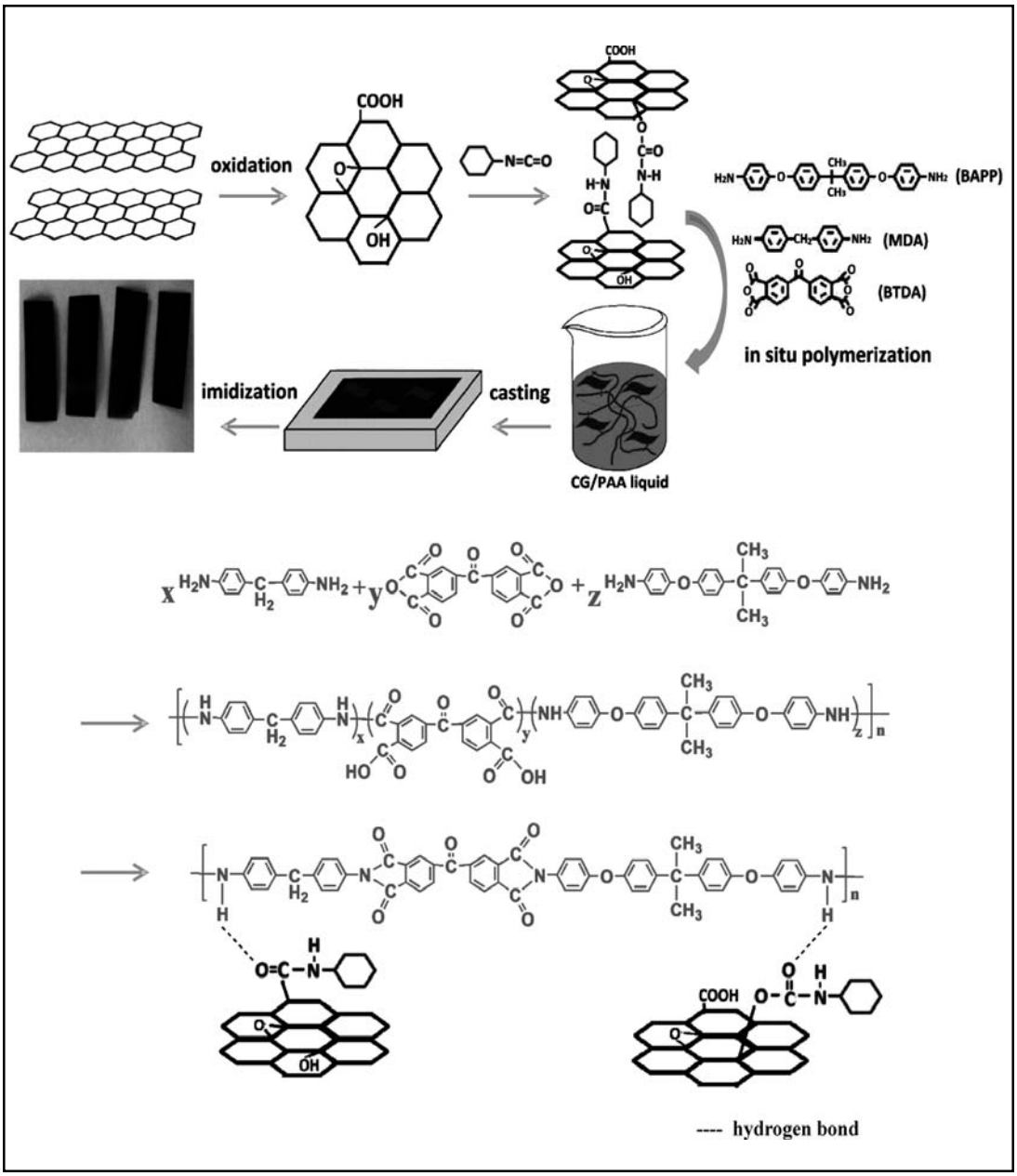

Fig. 1. The schematic representation of the synthesis and fabrication steps of cyclohexyl grafted graphene and the CG/PI composites

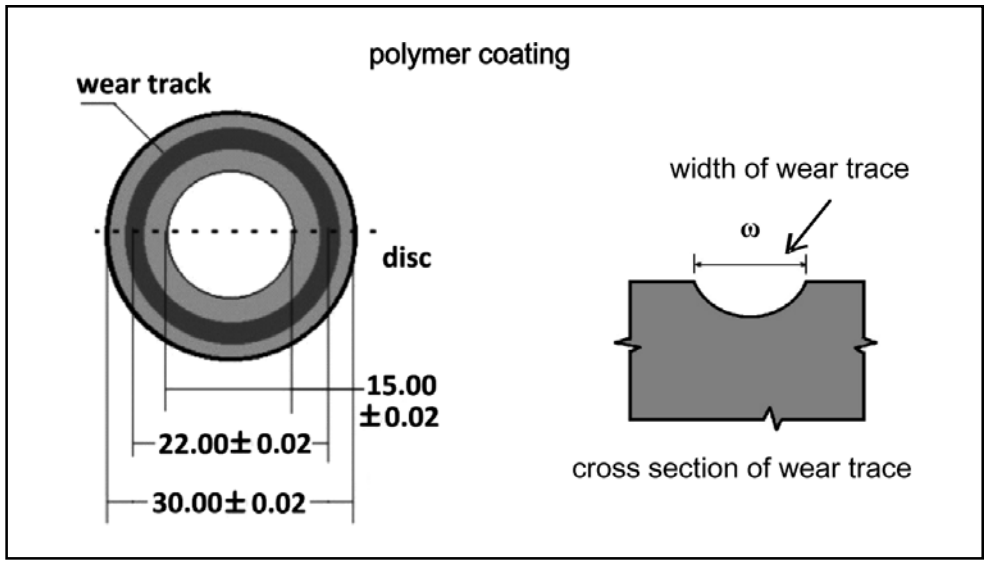

Fig. 2. The friction model of the ball-on-disc tribometer

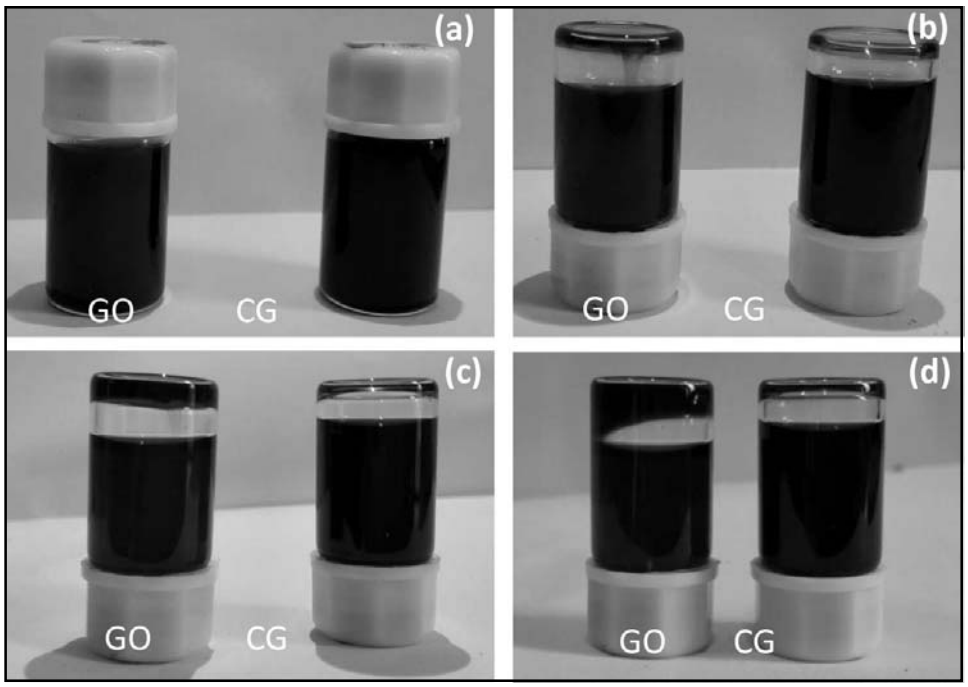

Fig. 3. Dispersion of GO and CG in 1.8 mg/mL of NMP (left for GO, right for CG) after ultrasonication in 0.5 h (a); 1 h (b); 24 h (c); 72 h (d)

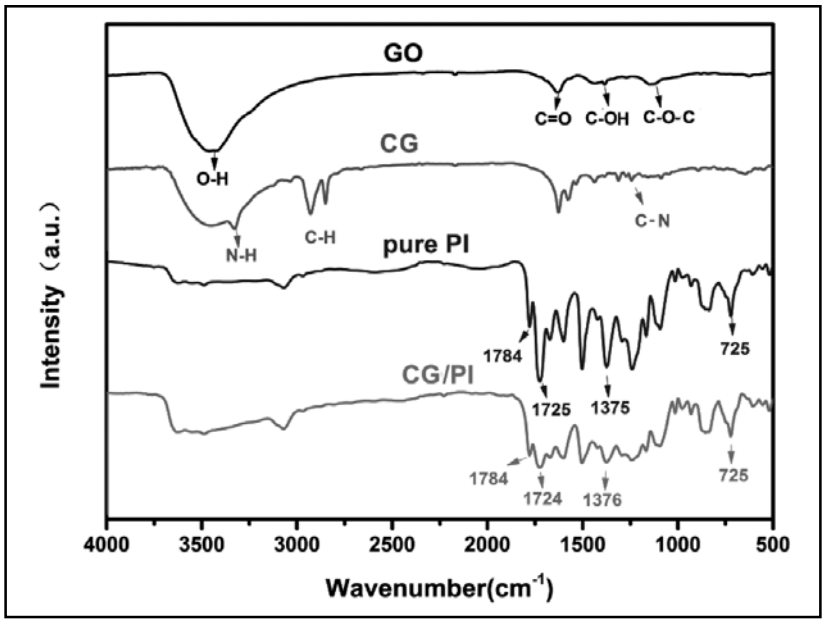

Fig. 4. FT-IR spectra of GO, CG, pure PI, and 0.5CG/PI composite

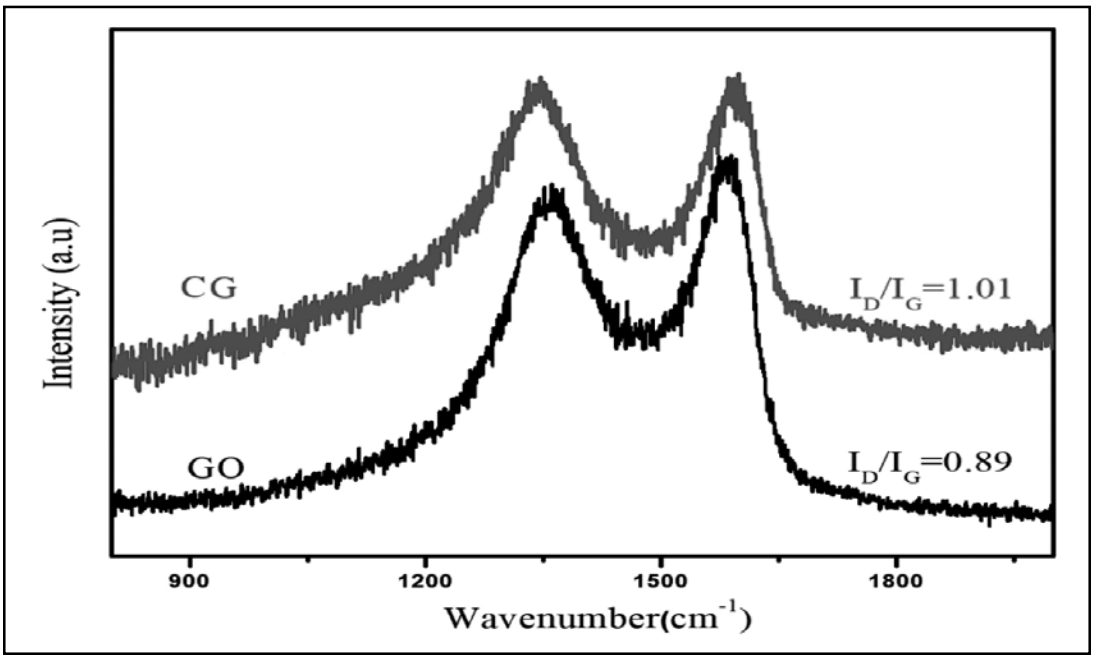

Fig. 5. Raman spectra of GO and CG

such as the peaks at 1243, 1545, 2852, 2921, 3328 cm^{-1}, were observed, which are assigned to the C–N stretching vibration, the –NH bending vibration, and the $–CH_2$ stretching symmetry vibrations and asymmetry vibrations, –NH stretching vibration, respectively. This indicated that on the GO sheet surface, chemical grafting reaction occurred between the CI molecules and the oxygen-containing functional groups.

The PI spectra show peaks at 725, 1375, 1725, and 1784 cm^{-1}, which belong to the C=O bending vibration, C-N-C axial stretching vibration, C=O symmetric stretching vibration, and C=O asymmetric stretching vibration, respectively. Similar peaks were also found in the spectra of the CG/PI composite, indicating that the incorporation of CG has no obvious effect on the reaction and thermal imidization during polyimide polymerization.

Raman spectroscopy is an important analytical method for non-destructive examination of carbon materials, and thus, it can characterize the structural changes of graphene [44, 45]. All Raman spectra of the samples presented in Fig. 5 show two broad peaks at approximately 1350 cm^{-1} for the D band and at 1580 cm^{-1} for the G band. The D band (disorder-induced Raman mode) is associated with the TO (transverse optical) branch near the K-point in the Brillouin zone, which arises from the breathing modes in the C=C ring structures, indicating the disorder degree [46]. The G band is associated with the doubly degenerate zone centre symmetry that allowed the E2g mode at the G point at the Brillouin zone centre,[47] which is assigned to the C (sp^2) –C (sp^2) bond stretching vibrations. The D bands of GO, and CG are located at 1348.7, 1346.1 cm^{-1}, which did not show obvious wavenumber shifts. However, the G bands of GO, and CG are located at 1578.3, 1584.6 cm^{-1}, which showed shifts to high wavenumber. Moreover, the ID/IG ratio (D-peak intensities/G-peak intensities), which is widely used to evaluate the disorder in graphene-based materials, did change obviously after the grafting. The ID/IG ratios of GO were found to be 0.89, while the ID/IG ratio of CG reached 1.01, indicating the incorporation of N heteroatoms of CG and successful reaction with the oxygen-containing group of GO.

X-ray diffraction spectra can be used to investigate the crystal and layered structure of graphene sheets. Fig.6 shows the XRD patterns of graphite, GO, CG, PI, and 0.5CG/PI composites. It is found that the (002) diffraction peak of graphite appears at $2\theta = 26.42°$, and the interlayer d-spacing (0.34 nm) is calculated by the Bragg equation, while the GO spectra showed the (001) diffraction peak at $2\theta=10.02°$ corresponding to 0.88 nm. The lower location of a diffraction peak of CG is 9.41°, corresponding to the interlayer spacing of 0.94 nm, which is larger than that of GO. This is mainly caused by two reasons: on the one hand, the introduction of a large-bulk ring group increases the CG layer spacing; on the other hand, the steric hindrance and organic groups weakened the van der Waals forces between layers, hindering the aggregation or lamination. In addition, the broad and weak peak of CG indicated that the crystallinity and the structural order decrease relative to GO. In particular, the peaks at approximately 21.01° in the CG patterns may be due to intense chemical reduction and re-stacking. However, the

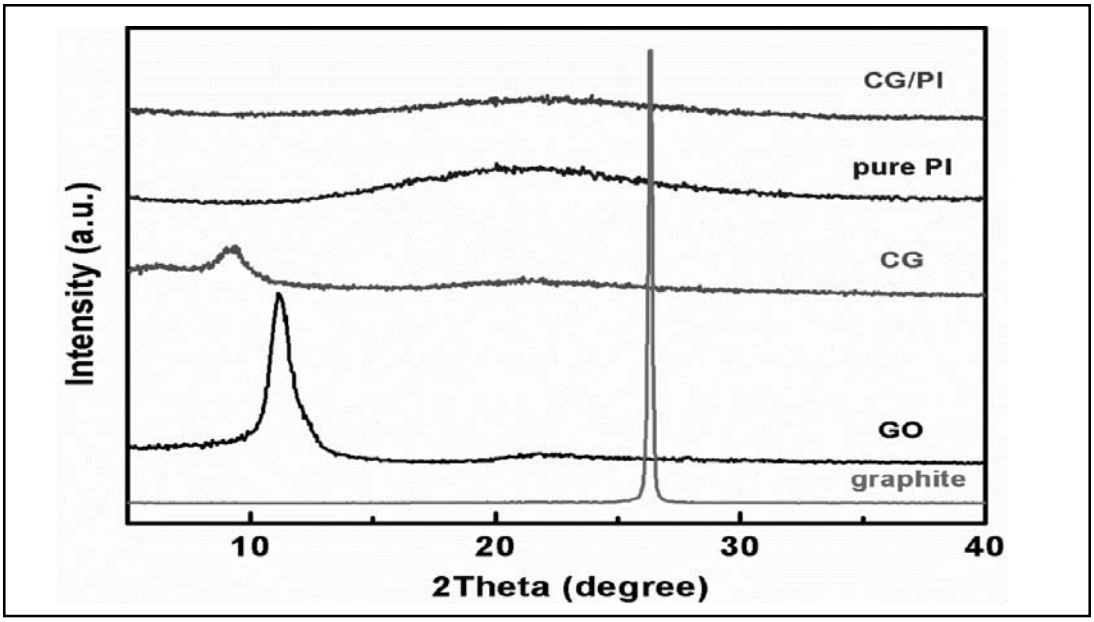

Fig. 6. X-ray diffraction spectra of GO, CG, pure PI, and CG/PI composite

characteristic (001) diffraction peaks are not found in the patterns of the CG/ PI composites, indicating that the CG are almost exfoliated further by in situ polymerization and are uniformly dispersed in the PI matrix. This result is in agreement with the results of our dispersion experiment in the NMP solution as described above.

TEM and AFM micrographs were recorded to observe the micro-morphology of graphene sheets and are shown in Fig. 7. It can be seen from the TEM images that both GO and CG are carpet-like and contain thin ripples and wrinkles, illustrating their similar structures. However, compared to GO, CG has more wrinkles, curled folds and dark transparency, which is attributed to the grafting of the CI organic chain. To further investigate the morphology of GO and CG, these sheets were ultrasonically dispersed in alcohol and then dropped onto clean mica sheets, and observed to be smaller than $3 \times 3\ \mu m^2$. Fig. 7d shows that the thickness of CG is 1.893 nm, greater than that of GO (1.673 nm). GO had a thin lamellae structure, while the lamellae of CG are thick, indicating that CI chains were successfully grafted onto GO sheet. This is consistent with the FT-IR analysis results.

Thermal gravimetric analysis (TGA) can be used to study the thermal stability and provide important information on the decomposition process of samples, such as the decomposition temperature and the residual content. According to the TGA curve in Fig. 8, CG showed a slight weight loss (4.8%) at 100 °C, while GO showed a weight loss of up to 16.2%, which is attributed to the pyrolysis of the crystal water on the surface of sheets. The

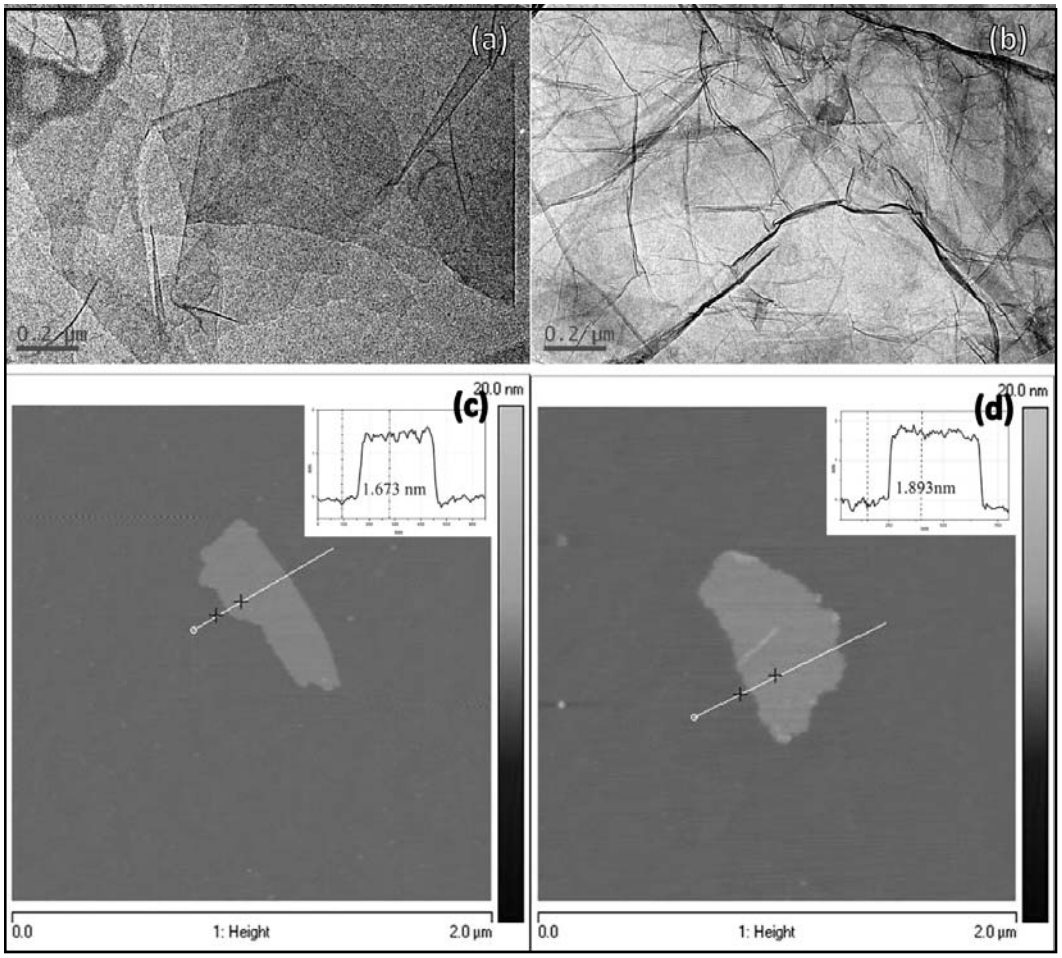

Fig. 7. TEM and AFM micrographs of GO (left) and CG (right)

great decrease of the CG surfacial hygroscopicity further demonstrated the successful modification and the change of surface energy and polarity after grafting of cyclohexyl isocyanate. In the 100~250 °C range, the weight loss of GO and CG reaches 25.7% and 20.3%, which is mainly caused by the thermal degradation of the oxygen-containing groups with the release of CO and CO_2. As the temperature increased further to 650 °C, GO showed almost no weight loss (7.4%), while CG showed 15.2% weight loss, owing to the pyrolysis of the doped organic functional groups [48]. The residual content of CG is 59.8%, obviously higher than that of GO (48.5%), further indicating that the thermal stability of the sheets is obviously improved by the surface modification.

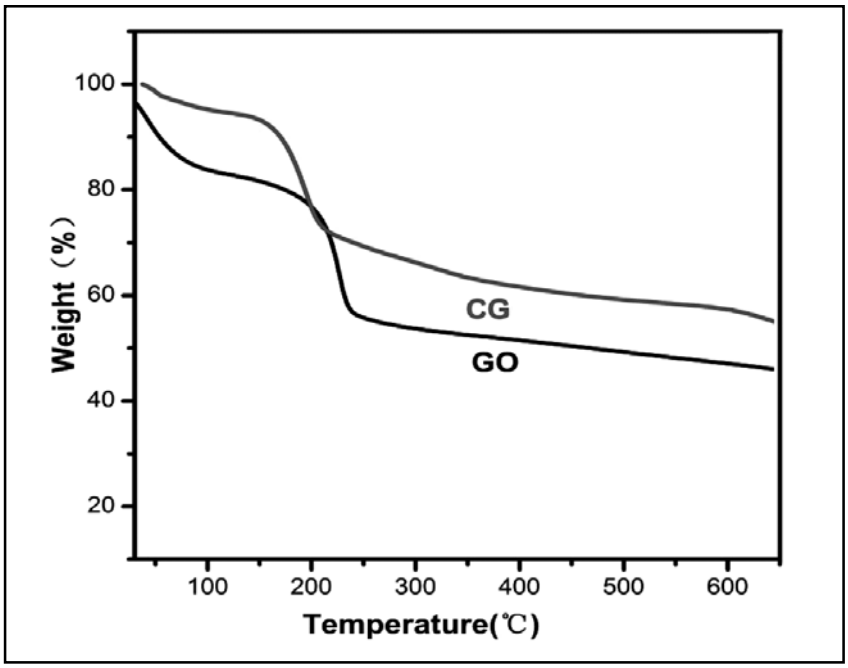

Fig. 8. TGA curves of GO and CG

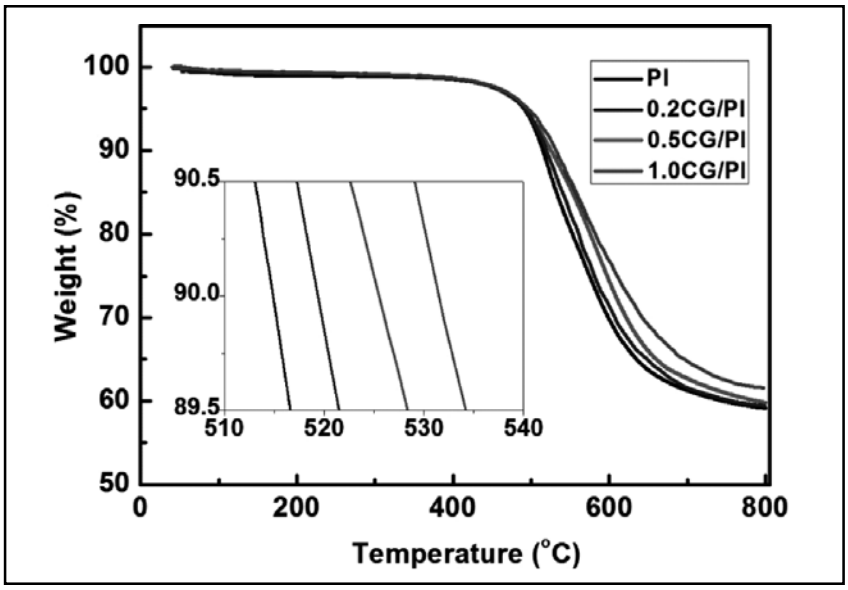

Fig. 9. TGA curves of PI and the CG/PI composites

TABLE 1. TGA data of PI and the CG/PI composites

0	neat PI	0.2CG/PI	0.5CG/PI	1.0CG/PI
T5% /°C	491.0	491.5	491.5	493.0
T10% /°C	515.0	519.0	525.5	531.5
Tmax /°C	564.5	568.5	588.5	593.0
Wr* /%	59.1	59.3	59.8	61.7

* Rw: percentage of residual weight at 800 °C

3.2. Preparation and characterization of CG/PI composite

According to previous reports, the enhancement effect of inorganic particles on the polymer modification often depends on the properties of the particles such as content, size, shape, dispersion, inorganic organic interface, interfacial stress transfer capacity and so on [49, 50].

The thermal stability of polyimide, as an engineering polymer applied under high temperature conditions, is an important property of the modified polyimide composites [51, 52]. The thermal stability of polymers is generally represented by the decomposition temperature, such as $T_{5\%}$, $T_{10\%}$, or Tmax, corresponding to the temperatures for 5% weight loss, 10% weight loss, and the maximum weight loss rate, respectively. As shown in Fig. 9 and Table 1, $T_{5\%}$, $T_{10\%}$ and Tmax of CG/PI composites increased with the CG content increasing. The $T_{10\%}$ of 1.0CG/PI reached 531.5 °C, increasing by 16.5°C from the pure PI (515.0 °C), while Tmax of CG/PI reached 593.0 °C, increasing by 28.5°C from the pure PI (564.5 °C). Furthermore, the percentage of residual weight of CG/PI was higher than pure PI. Thus the thermal stability of CG/PI has been significantly improved compared to that of the pure PI. This improvement may because of three main points: first, the modified graphene enhanced the compatibility between the sheets and PI matrix. The hydrogen bonding between the amide groups of CG and PI chain lead to a good interfacial interaction between the two phases; second, the two-dimensional layered structure with the large diameter-thickness ratio of CG evenly exist in the polymer matrix to form a percolation network with a “tortuous release path”, which can effectively restrict or delay the diffusion and escape of oxygen and other unstable molecules. Finally, the high thermal conductivity of CG results in effective heat dissipation, thereby reduces or avoids heat accumulation and retards the thermal degradation. The synergistic effect of these factors can significantly improve the thermal stability of the CG/PI composites.

Mechanical properties of the pure PI and the CG/PI nanocomposites were measured on a universal testing machine and showed in Table 2. The properties were obtained as the average values of five experimental measurements. It can be seen that the tensile strength and the Young’s modulus of the CG/PI nanocomposites is uptrend with the increase of CG content. The Young’s modulus of the 1.0CG/PI nanocomposite reached 99.35 MPa

TABLE 2. Mechanical properties of PI and CG/PI composites

	neat PI	0.2CG/PI	0.5CG/PI	1.0CG/PI
Tensile strength /Mpa	82.13	86.92	96.72	99.35
Young's modulus /Gpa	1.43	1.53	1.70	1.84
Elongation at break /%	13.84	11.89	9.31	7.95

and 1.84 GPa, respectively, 20.97 % and 28.67 % higher than the values obtained for the pure PI (82.13 MPa, 1.43 GPa). The mechanical properties of the CG/PI nanocomposites shows a significant improvement, compared to that of pure PI. This may be owing to the CG surrounded by an organic shell is evenly dispersed in the matrix with good interface bonding. Furthermore, the inorganic-organic compatibility by hydrogen bonds is improved, and the physically cross-linked sheets effectively inhibit or resist the formation of tensile shear bands and the propagation of shear micro-cracks. Therefore, the incorporation of CG can significantly improve the mechanical properties of polyimide-based composites. However, the elongation at break of the CG/PI composites decreased with the loading of CG increasing, and the all CG/PI composite still appeared brittle fracture before reaching the yield strength. This is mainly because the CG, as the "interlock point", blocked the macromolecule segments and made PI chains' relative movement difficult, resulting in the brittle deformation.

To study the mechanism of the improved interface and dispersion, we observed the fractured surfaces of the pure PI and of the 1.0CG/PI composite films by SEM, as shown in Fig. 10. It can be seen from Fig. 10a that the fractured surface of the pure PI is relatively smooth and bare, and the cracks are relatively rare, showing a typical brittle fracture. Fig. 10b shows that the fractured surface of the CG/PI composite exhibits a more complex morphology that is relatively rough and irregular. However, the sheets are uniformly dispersed in the matrix. CG sheets, as the stress concentration body, initiate and terminate the micro-cracks and bear the main external forces. Moreover, the good interface bonding make the external energy effectively transferring between the matrix and the sheets to maximize the enhancement effect [53]. The fracture morphology of the pure PI and CG/PI further supports the important correlation between the mechanical properties and the microstructure of the materials.

3.3. Tribological properties of the CG/PI composite

The tribological properties of polymer are usually related to the mechanical properties and thermal properties, making it difficult to detach debris from the worn surface of the polymer [54]. To systematically study the effects of CG sheets on the tribological properties of the CG/PI composites, dry-friction test was carried out at a speed of 0.628 m/s with a load of 5 N at room temperature, and the results are shown in Fig. 11 and Table 3.

The curves of PI or CG/PI nanocomposites showed that the friction behaviour exhibited a run-in period at first and a stable period later. At the initial stage of the friction process, the

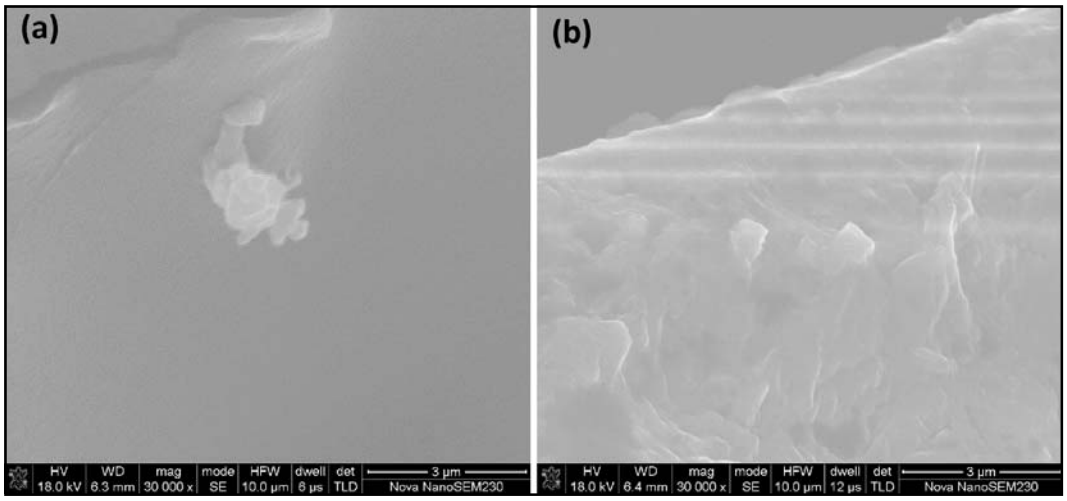

Fig. 10. SEM micrographs of the brittle fracture surface of the pure PI (a) and CG/PI composite (b)

friction coefficients of all samples increased owing to the asynchronous effect of cutting, collision and plastic deformation of the contact surfaces. As the friction process continues, the bulges are rubbed down by polishing, and the caves are filled. The frictional contact area increases and the transfer film is stably formed and adhered. Finally, more and more CG sheets was exposed, oriented and tiled, reduced and stabilized the friction coefficient as a solid lubricant. As shown in Table 3, both friction coefficient and wear rate of CG/PI composites showed the downtrend along with the increasing content of CG. The friction coefficient of 1.0CG/PI was 0.35, lower than that of the pure PI (0.52), decreased by 32.69 %. The wear rate of 1.0CG/PI also reached 3.07×10^{-5} mm^3/Nm, corresponding to the 29.10 % decrease relative to the pure PI (4.33×10^{-5} mm^3/Nm). As the CG incorporated, the friction coefficient and wear resistance of CG/PI composites had a significantly enhancement compared to pure PI.

This enhancement is caused by the incorporation of CG in the PI matrix, which can be reinforced, thermo-stabilized and lubricated. Another reason may be that with CG's good thermal conductivity. The CG sheets were beneficial for thermal rapid dissipation in the matrix and prevented the performance at the high temperature from reducing. Moreover, CG can make transfer films on the surface of the metal spheres formed and reduce the adhesion wear and the friction coefficient. However, pure PI is prone to being stripped off, showing the poor friction performance.

To analysis the frictional mechanism of polymer materials, a morphology analysis of the wear surface was performed using SEM. As shown in Figure 12, the wear surface of pure PI shows more cracks, an uneven distribution, and large area peeling, indicating that the main wear included adhesive wear and fatigue wear. However, the wear surface of the 1.0CG/PI composite is relative even and flat, with only a few rubbing marks and minor

scratches, showing mainly adhesive wear and slight abrasive wear. All factors, including friction force, load pressure, electrostatic force, van der Waals forces and hydrogen bonds, affects the friction behaviour. Thus, the frictional surface material of polymer undergoes plastic deformation and transfers to the metal surface to form a transfer film and inhibit from excessive scratching that causes adhesive wear[55]. After the incorporation of the modified graphene into the polymer matrix, the modified nanosheets were bonded and covered tightly with the polymer shell because of good surface bonding and even dispersion, and thus, they can greatly reinforce the surficial material and reduce the plastic deformation of inner materials [56]. In summary, cyclohexyl isocyanate modified graphene, reinforced and thermal-stabilized PI material and lubricate plastic and sliding metal parts, and remarkably reduced friction coefficient and enhanced the wear resistance of the PI composites.

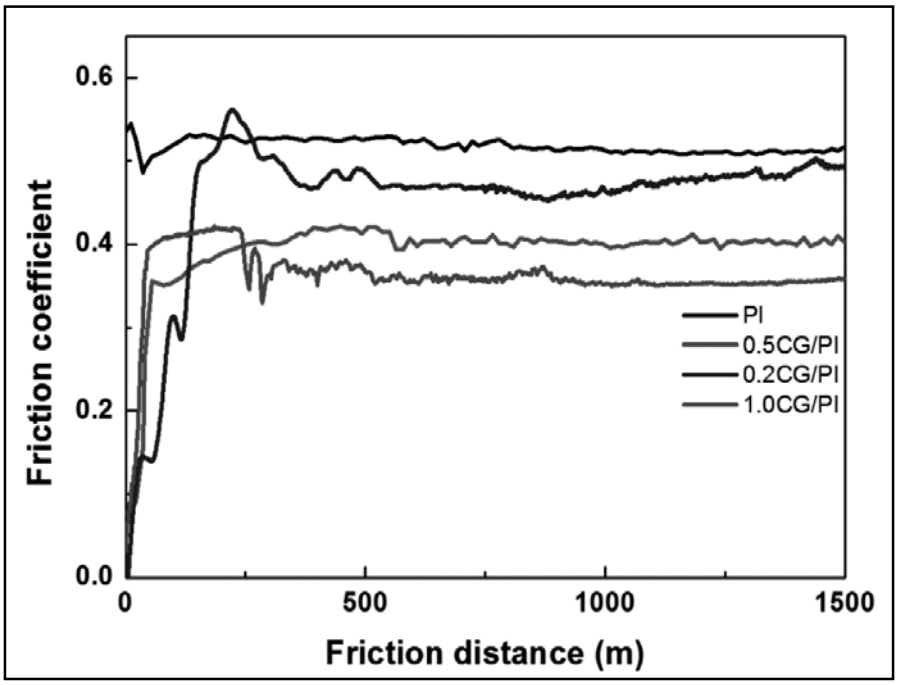

Fig. 11. Friction curves of pure PI and CG/PI composites

TABLE 3. Tribological properties of pure PI and CG/PI composites

0	**neat PI**	**0.2CG/PI**	**0.5CG/PI**	**1.0CG/PI**
Friction coefficient	0.52	0.48	0.40	0.35
Wear rate $\times 10^{-5}$ mm^3/Nm	4.33	3.91	3.29	3.07

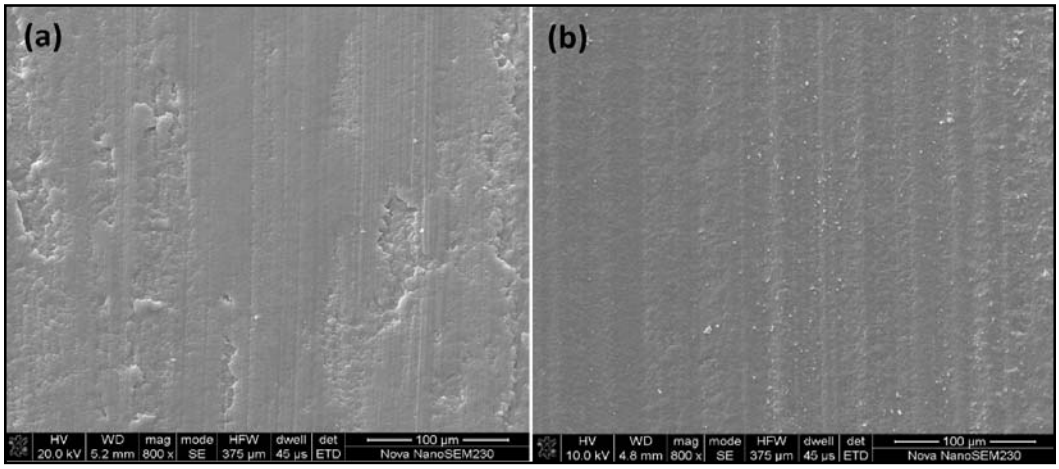

Fig. 12. SEM micrographs of the friction surface of pure PI (a) and CG/PI composite (b)

CONCLUSIONS

In this work, cyclohexyl isocyanate modified graphene was prepared and used to synthesize a series of CG/PI composites by in situ polymerization. After graphene sheets grafted by cyclohexyl isocyanate, their interlayer spacing increased, and the compatibility and dispersion in the PI matrix were modified significantly. Furthermore, compared to pure PI, the mechanical and thermal stability of the CG/PI nanocomposites were enhanced. The tensile strength and Young's modulus of the 1.0CG/PI nanocomposite reached 99.35 MPa and 1.84 GPa, increased by 20.97 % and 28.67 %, respectively, compared with pure PI. The friction coefficient and the wear rate of the 1.0CG/PI composite reached 0.35 and 3.07×10^{-5} mm^3/Nm, respectively, which decreased by 32.69 % and 29.10 % compared with pure PI. CG markedly enhanced tribological properties of polyimide composites. CG, acting as a reinforcer, thermal-stabilizer and lubricant, markedly reduced the friction coefficient and wear rate of the polyimide composites. The excellent improvement of these polyimide materials has an important value for the development and application of graphene /polymer composites.

REFERENCES

1. Dai W, Yu J, Liu Z, et al. *Compos Part A-Appl S* 2015; 76: 73-81.
2. Cao L, Sun Q, Wang H, et al. *Compos Part A-Appl S* 2015; 68: 140-148.
3. Fang X, Liu X, Cui ZK, et al. *J Mater Chem A* 2015; 3: 10005-10012.
4. Jia Z, Hao C, Yan Y, et al. *Wear* 2015; s 338–339: 282-287.
5. Ye X, Liu X, Yang Z, et al. *Compos Part A-Appl S* 2016; 81: 282-288.
6. Chang J, Niu H, Zhang M, et al. *J Mater Sci* 2015; 50: 4104-4114.
7. Johnson RL, Lee J and Loomis WR. *Hydraulics & Pneumatics* 1970; 23: 130.

8. Sun C, Feng Z, Lei S, et al. *Appl Surf Sci* 2006; 253: 1729-1735.
9. Jia JH, Zhou HD, Gao SQ, et al. *Mat Sci Eng A-Struc* 2003; 356: 48-53.
10. Zhang XR, Pei XQ and Wang QH. *Mater Design* 2009; 30: 4414-4420.
11. Wang Q, Zhang X and Pei X. *Mater Design* 2010; 31: 3761-3768.
12. Samyn P, Schoukens G, Quintelier J, et al. *Tribology International* 2006; 39: 575-589.
13. Lv M, Zheng F, Wang Q, et al.*Tribology International* 2015; 92: 246-254.
14. Song F, Wang Q and Wang T. *Compos Sci Technol* 2016; 134: 251-257.
15. Zhao Y, Qi X, Dong Y, et al. *Tribology International* 2016; 103: 599-608.
16. Nayak L, Rahaman M, Khastgir D, et al. *J Appl Polym Sci* 2017: 45862.
17. Kwon K and Chang JH. *J Compos Mater* 2014; 49: 3031-3044.
18. Li TL and Hsu LC. *J Phys Chem B* 2010; 114: 6825.
19. Yang S, Choi J and Cho M. *ACS Appl Mater Interfaces* 2012; 4: 4792.
20. And MM and Winey KI. *Macromolecules* 2006; 39: 543-545.
21. Chen Y and Iroh JO. *Chem Mater* 1999; 11: 1218-1222.
22. Allen MJ, Tung VC and Kaner RB. *Chem Rev* 2010; 110: 132.
23. Shao Y, Wang J, Wu H, et al. *Electroanalysis* 2010; 22: 1027-1036.
24. Wang F, Drzal LT, Yan Q, et al. *J Mater Sci* 2015; 50: 1082-1093.
25. Choi W, Lahiri I, Seelaboyina R, et al. *Crit Rev Solid State Mater Sci* 2010; 35: 52-71.
26. Penkov O, Kim HJ, Kim HJ, et al. *Int J Precis Eng Man* 2014; 15: 577-585.
27. Novoselov KS, Geim AK, *Science* 2004; 306: 666.
28. Chen Y, Wang Y, Zhang HB, et al. *Carbon* 2015; 82: 67-76.
29. Wan YJ, Yang WH, Yu SH, et al. *Compos Sci Technol* 2016; 122: 27-35.
30. Zeng H, Zhu X, Liang Y, et al. *Polymers* 2015; 7: 333-372.
31. Macosko C. *Macromolecules* 2010; 43: 6515-6530.
32. Kuilla T, Bhadra S, Yao D, et al. *Prog Polym Sci* 2010; 35: 1350-1375.
33. Liu K, Chen L, Chen Y, et al. *J Mater Chem* 2011; 21: 8612-8617.
34. Zaman I, Kuan HC, Meng Q, et al. *Adv Funct Mater* 2012; 22: 2735-2743.
35. Valentini L, Cardinali M, Bon SB, et al. *J Mater Chem* 2010; 20: 995-1000.
36. Ramanathan T, Abdala AA, Stankovich S, et al. *Nat Nanotechnol* 2008; 3: 327-331.
37. Lin P, Meng L, Huang Y, et al. *Appl Surf Sci* 2015; 324: 784-790.
38. Li J, Wang F and Liu CY. *J Colloid Interface Sci* 2012; 382: 13.
39. Stankovich S, Piner RD, Nguyen SBT, et al. *Carbon* 2006; 44: 3342-3347.
40. Zhao H, Wu L, Zhou Z, et al. *Phys Chem Chem Phys* 2013; 15: 9084.
41. Ramezanzadeh B, Ghasemi E, *Chem Eng J* 2015, 281: 869-883.
42. Wang T, Cheng C, Wu L, et al. *Environ Sci Technol* 2017; 51.
43. Hummers WS and Offeman RE. *J Am Chem Soc* 1958; 80: 1339.
44. Xiang Q, Yu J and Jaroniec M. *Nanoscale* 2011; 3: 3670-3678.
45. Lunghao HB, Wu FY, Lin CT, et al. *Nat Commun* 2013; 4: 1687.

46. Rao CNR, Sood AK, Subrahmanyam KS, et al. *Angew Chem Int Edit* 2009; 48: 7752–7777.

47. Ferrari AC, Meyer JC, Scardaci V, et al. The Raman Fingerprint of Graphene. 2006.

48. Hsiao MC, Liao SH, Yen MY, et al. *ACS Appl Mater Interfaces* 2010; 2: 3092-3099.

49. Yuan QW, Kloczkowski A, Mark JE, et al. *J Polym Sci Pol Phys* 2015; 34: 1647-1657.

50. Hassanabadi HM and Rodrigue D. *Macromol Mater Eng* 2015; 299: 1220-1231.

51. Turk MJ, Ansari AS, Alston WB, et al. *J Polym Sci Pol Chem* 2015; 37: 3943-3956.

52. He L, Zhang P, Chen H, et al. *Polym Int* 2016; 65: 84-92.

53. Zhang YM, Zhang WG, Fan M, et al. *Acta Mech* 2016; 228: 1-16.

54. Myshkin NK, Petrokovets MI and Kovalev AV. *Tribol Int* 2006; 38: 910-921.

55. PhilAttard. *J Adhes Sci Technol* 2002; 16: 753-791.

56. Timin AS, Khashirova SY, Zhansitov A, et al. *Colloid Polym Sci* 2015; 293: 1667-1674.

Received: 15-01-2018

Accepted: 15-03-2018